Biogeosciences Discuss., 7, 165–202, 2010
www.biogeosciences-discuss.net/7/165/2010/

Biogeosciences Discussions

This discussion paper is/has been under review for the journal Biogeosciences (BG).
Please refer to the corresponding final paper in BG if available.

Trends of anthropogenic CO_2 storage in North Atlantic water masses

F. F. Pérez[1], M. Vázquez-Rodríguez[1], H. Mercier[2], A. Velo[1], P. Lherminier[2], and A. F. Ríos[1]

[1]Instituto de Investigaciones Marinas, CSIC, Eduardo Cabello 6, 36208 Vigo, Spain
[2]Laboratoire de Physique des Océans, CNRS Ifremer IRD UBO, IFREMER Centre de Brest, B.P. 70 29280 Plouzané, France

Received: 29 November 2009 – Accepted: 24 December 2009 – Published: 13 January 2010

Correspondence to: F. F. Pérez (fiz.perez@iim.csic.es)

Published by Copernicus Publications on behalf of the European Geosciences Union.

Abstract

A high-quality inorganic carbon system database spanning over three decades (1981–2006) and comprising 13 cruises has allowed applying the φC_T° method and coming up with accurate estimates of the anthropogenic CO_2 (C_{ant}) stored in the main water masses of the North Atlantic. In the studied region, strong convective processes convey surface properties, like C_{ant}, into deeper ocean layers and confer this region an added oceanographic interest from the point of view of air-sea CO_2 exchanges. Commonly, a tendency for decreasing C_{ant} storage rates towards the deep layers has been observed. In the Iberian Basin, the deep waters (North Atlantic Deep Water) have low C_{ant} values and negligible C_{ant} storage rates, while the North Atlantic Central Water in the upper layers shows the largest C_{ant} concentrations and capacity to increase its storage on a yearly basis ($1.13\pm0.14\,\mu mol\,kg^{-1}\,yr^{-1}$). This unmatched C_{ant} storage capacity of the warm upper limb of the Meridional Overturning Circulation weakens towards the Irminger basin ($0.68\pm0.06\,\mu mol\,kg^{-1}\,yr^{-1}$) due to the lowering of the buffering capacity. The mid and deep waters in the Irminger Sea show rather homogeneous C_{ant} storage rates (between 0.33 and $0.45\,\mu mol\,kg^{-1}\,yr^{-1}$), whereas in the Iceland basin these layers seem to have been less affected by C_{ant}. The C_{ant} storage rates in the study region during the 1991–1997 high NAO (North Atlantic Oscillation) phase are ~48% higher than during the 1997–2006 low NAO phase that followed. This result suggests that a net decrease in the strength of the North Atlantic sink of atmospheric CO_2 has taken place during the present decade. The changes in deep-water ventilation together with a detrimental renewal of the main water masses are likely the main driving processes causing this weakening of the North Atlantic CO_2 sink.

1 Introduction

The North Atlantic is known as the most important CO_2 sink of the global ocean (Sabine et al., 2004). Recent studies and future scenarios from the International Panel on Cli-

BGD

7, 165–202, 2010

mate Change (IPCC, 2007) point towards a decline in the intensity of the Meridional Overturning Circulation (MOC) in the next 100 years. The causes for it are mainly attributed to the greenhouse-enhanced temperature rise and freshwater fluxes in the high latitudes, where water mass formation processes abound. The slowdown of MOC would bring forth profound consequences for global climate due to the associated decrease in heat transport (Drijfhout et al., 2006) and oceanic anthropogenic CO_2 (C_{ant}) uptake (Sarmiento and Le Quéré, 1996).

The Labrador Sea Water (LSW) is one of the thickest water masses in the North Atlantic, and one of the main components of the lower limb of MOC that flows southwards. Several Ocean General Circulation Models (OGCMs) have suggested that the decadal variability of the MOC is closely related with the variability of LSW formation rates (Latif et al., 2006; Böning et al., 2006; Steinfeldt et al., 2009).

The water column stratification and wind forcing intensity are determinant factors in the efficiency of convective processes (Dickson et al., 1996; Curry et al., 1998; Lazier et al., 2002). Convection activity in the Labrador Sea is related to the persistence and phase of the North Atlantic Oscillation (NAO). A positive NAO phase causes stronger winds and heat loss in the Labrador Sea, fostering convection. During the early 1990's, the highly positive phase of the NAO matched with an impressive and exceptional convection activity down to more than 2000 m (Dickson et al., 1996; Lazier et al., 2002; Häkkinen et al., 2004; Yashayaev et al., 2008). This resulted in the formation of the thickest layer of classical LSW (cLSW) observed in the past 60 years (Curry et al., 1998). This high LSW formation period that started in 1988 (Sy et al., 1997) ended abruptly in 1996 with the shift from high to a low NAO phase. Nonetheless, weaker convection events (to less than 1000 m depth on average) continued to take place in the central Labrador Sea and formed the less dense upper LSW (uLSW).

The present work examines the temporal variability of C_{ant} storage in the main water masses of the North Atlantic (>40° N). This region is a fast-track entrance portal for C_{ant} to the deep ocean through the overturning circulation caused by deep convection (Kieke et al., 2007; Pérez et al., 2008). By applying the φC_T° C_{ant} estimation method

(Vázquez-Rodríguez et al., 2009a), the aim is to study and quantify the changes in C_{ant} storage rates that occurred in the North Atlantic since the early 1980s. The changes can be provoked by the actual changes in the amounts of C_{ant} that are being stored in the ocean (as a direct consequence of rising atmospheric CO_2 levels) and by the changes in the volumetric census of the main water masses involved in this region (Steinfeldt et al., 2009). These two processes will be evaluated in this work.

2 Dataset

A total of thirteen cruises with high-quality carbon system measurements were selected to follow the temporal evolution of C_{ant} in the North Atlantic. The combined dataset spans over 25 years (1981–2006) and gives a comprehensive spatial coverage of the area (Fig. 1a; Table 1), with an emphasis on important water mass transformation areas like the Irminger and Iceland basins. The geographical boundaries of the Irminger basin have been established between the main axis of the Reykjanes Ridge and the east coast of Greenland (Fig. 1a). Likewise, the Iceland basin is defined as the region enclosed between the Reykjanes Ridge axis and the line joining the Eriador Seamount and the Faroe Islands. The region designated as Eastern North Atlantic basin (ENA basin hereinafter) extends south from the Eriador-Faroe line over the Rockall trough, the Porcupine bank, and the Biscay and Iberian basins.

Only bottle data that included carbon system analysis were used in this study. Some of the older cruises here considered could not possibly use certified reference materials (CRMs) for their carbon system measurements in the year they were conducted. Also, the determination procedures varied between cruises, especially before Oaces in 1993. These differences in the analytics have an effect on the precision attainable for a given carbon variable. In any case, the high quality of carbon measurements was one of the main criteria considered for cruise selection, i.e., all data are compliant with the latest carbon system analytical recommendations for seawater (DOE, 1994). They were accessed from the Carbon In the Atlantic (CARINA) data por-

tal (http://store.pangaea.de/Projects/CARBOOCEAN/carina/index.htm), except for the OVIDE '06 and OVIDE '08 data.

The annual averages from the World Ocean Atlas 2005 climatology (WOA05; http://www.nodc.noaa.gov/OC5/WOA05/woa05data.html) have been additionally used as references for normalizing layer thicknesses and tracer concentrations to basin-wide averages, given the heterogeneous and eventually sparse spatial coverage in some areas (Fig. 1a). This has occurred in spite of having used a comprehensive number of thirteen cruises that meet the desired data quality for the carbon system and provide good temporal coverage at the same time. The WOA05 database provides annual, seasonal and monthly averages of several tracers for grid resolutions of 1°×1° and 5°×5° over 33 depth levels. In this study we have used the annual average with 1°×1° grid resolution.

The pH was determined either potentiometrically (Dickson, 1993a,b) using pH electrodes or, more commonly, with a spectrophotometric method (Clayton and Byrne, 1993) adding *m*-cresol purple as the indicator in either scanning or diode array spectrophotometers. The spectrophotometric pH determination has typical precision limits of 0.002 pH units (Clayton and Byrne, 1993; Millero, 2007). Exceptionally, the pH measurement protocols of the FOUREX and OVIDE cruises included periodical CRM checks that allowed achieving a precision of 0.0014.

All shipboard A_T samples were analyzed with potentiometric titration and determined by developing either a full titration curve (Millero et al., 1993; DOE, 1994; Ono et al., 1998) or from single point titration (Pérez and Fraga, 1987; Mintrop et al., 2002). The C_T samples were analyzed with Single Operator Multiparameter Metabolic Analyzers (SOMMA apparatus) based on coulometric titration techniques (Johnson et al., 1993) and calibrated with CRMs. The exception to the latter is the 1981 TTO cruise, where C_T was determined potentiometrically (Bradshaw et al., 1981) and no CRMs were used. The analytical accuracies for C_T, A_T and pH were equal to or better than ±2 µmol kg^{-1}, ±4 µmol kg^{-1} and ±0.003 pH units, respectively. As specified in Table 1, an analysis exercise performed by the Carboocean Atlantic Synthesis group examined all existing

Atlantic cruise crossovers and, for a few cruises, suggested corrections to the carbon system dataset (Pierot et al., 2009; Velo et al., 2009a,b).

The AR07E and A01E cruises deserved special treatment: they both had comprehensive amounts of coulometric C_T measurements but very few potentiometric A_T data. The geographic position and timely date of these two cruises made them assets to this study so as to discard them because of the sparseness in A_T data. Hence, a regression for normalized A_T ($NA_T = A_T \cdot 35/S$) was obtained from a NA_T vs. $Si(OH)_4$ (silicate) scatter plot that included all valid A_T measurements in the dataset below 100 m depth. This practice is justified given the low variability of A_T in the North Atlantic (Friis et al., 2005), and yielded a satisfactory NA_T fit as a function of silicate ($NA_T = 2294.7 + 1.37 \cdot Si(OH)_4$; $R^2 = 0.97$ and standard deviation of residuals of $\pm 3.7\,\mu mol\,kg^{-1}$). The obtained equation for the fit was then applied to the AR07E and A01E datasets to generate A_T values at the 3-D grid nodes of measured C_T.

3 Methodology

The high convection activity and C_{ant} sequestration capacity of the studied area motivated a water mass approach to successfully fulfil the aims of this work. In practice, following a particular set of water masses and studying their carbon system temporal variability has several advantages. Most importantly, this *modus operandi* avoids all the caveats common in closed volume, basin-wide approaches that encapsulate and treat equally very different water masses in terms of their relative "weight" or importance. In this sense, we have divided the observed hydrographical variability in the study area into its constituent and predominant water masses so that the variability of properties within each defined layer (Fig. 1b) remains minimum (Table 2). While mixing between water masses still occurs, the observed temporal changes of their properties are mainly attributed to water mass formation conditions. This same strategy has been successfully used in the past by various authors (Azetsu et al., 2003; Kieke et al., 2007; Sarafanov et al., 2007; Pérez et al., 2008).

Also, this layer approach allows a better extrapolation of the observed water mass properties during a particular cruise to the rest of the basin. This way, the need of considering unrealistic constant mean penetration depths (MPD) throughout the entire basin is avoided. On the other hand, our approach makes possible an evaluation of the thickness variability for each water mass, which is much more realistic and will improve considerably C_{ant} inventory estimates, as discussed later in this section.

The limits of the principal water masses identified in a TS diagram were set to ad hoc isopycnals selected in the Irminger, Iceland and ENA basins (Fig. 1b; Table 2). For the sake of consistency, the potential density (σ, in kg m^{-3}) limits suggested in previous works (Kieke et al., 2007; Yashayaev et al., 2008) were adopted, whenever possible.

The concentrations of C_{ant} shown in Fig. 2 (and in the rest of cruises, not plotted) have been estimated by applying the φC_T° method (Vázquez-Rodríguez et al., 2009a). The φC_T° method is a process-oriented geochemical approach that attempts to account for the nature and evolution of the phenomena that ultimately have affected the C_{ant} storage in the ocean since the 1750s. From the biogeochemistry of the marine carbon cycle to the mixing and air-sea exchange, it considers processes that control the uptake of C_{ant} by the ocean. It also considers the spatiotemporal variability since the pre-industrial era of the A_T° and ΔC_{dis} terms. The subsurface layer reference for water mass formation (WMF) conditions has served to produce high-performance parameterizations of A_T° and ΔC_{dis} that can be used to estimate C_{ant} without the need of any additional and arbitrary zero-C_{ant} references. Overall, the proposed method upgrades translate into significant impacts on C_{ant} inventories and bring closer together the estimates obtained from classical C_T°-based methods and newly introduced C_{ant} calculation approaches like the TrOCA or the TTD (Vázquez-Rodríguez et al., 2009b).

In order to calculate the inventories of C_{ant} and study their temporal variability trends, a few considerations on how this calculation has been done in previous studies must be brought forward. The classical way to calculate inventories requires vertically integrating the C_{ant} concentrations over the entire water column of the considered area. Assuming a transient steady state (Keeling and Bolin, 1967) for C_{ant} (Tanhua et al.,

2006), the mean penetration depth (MPD) is defined as the quotient between the specific inventory of C_{ant} in the water column and the C_{ant} concentration in the winter mixed layer. The works from Holfort et al. (1998), Roson et al. (2003) or Álvarez et al. (2004) have approximated the C_{ant} storage rates as the product of the time derivative of the average C_{ant} concentration in the winter mixed layer ($\partial C_{ant}^{WML}/\partial t$) times the MPD. The basis for this approximation relies on the fact that MPD is taken as constant, after the work from Broecker et al. (1979). However, Pérez et al. (2008) pointed out that the time variability of the MPD can affect notoriously C_{ant} storage rates, especially during high NAO phase time periods in or close to areas of water mass formation.

The latter approximation of a constant MPD basically does not contemplate basically does not contemplate the changes in the volumetric census of the water masses caused by differential formation rates in different years, which has been shown to be particularly the case in the Irminger and Iceland basins (Fig. 2). The deviations from the constant MPD assumption propagate into the inventory estimates, adding larger uncertainties and biases to them. The works from Kieke et al. (2006) and Steinfeldt et al. (2009), which calculated CFC inventories in the North Atlantic, had both pointed out the importance of considering the variability in the volumetric census of the water masses involved for inventory calculation purposes. They showed that the detected changes in the CFC inventories were largely produced by the changes in layer thickness of uLSW and cLSW.

To obtain more accurate specific inventories of C_{ant}, we have considered the variability of the layer thicknesses (Th hereinafter). The Th has been calculated as the average vertical distance between layers, weighed by the separation between stations. The averages for the rest of properties were computed integrating vertically and horizontally, and then dividing by the section area of the corresponding layer. The average thicknesses and layer properties are listed in Table 2. We have considered two different sets of thickness data, namely: Th calculated from different cruises over the same basin (denoted by "observed" thickness in Table 2) and also the thickness calculated from climatological data for the same cruise track (denoted by "WOA05" thickness in

Table 2). The ratio of these two "Th" (Eq. 2) compares the layer thickness observed during the cruises with that calculated from WOA05 data for the same cruise track. This procedure provides a real evaluation of the water mass formation variability by following the temporal evolution of the layer thicknesses. Considering the variability of the Th term also ensures a larger precision in storage rate evaluations. Properly harnessing down this term has an added value in closed box studies that aim at gauging balance transports across oceanic sections (Holfort, 1998; Roson et al., 2003; Álvarez et al., 2004) and for calculating C_{ant} air-sea fluxes by looking at the difference between the in-and-out net transport balances and the storage in a closed volume (convergences–divergences) of seawater (Mikaloff-Fletcher et al., 2006). These works have considered a constant MPD when calculating storages, unlike it will be done in the present study.

The inventory of C_{ant} for a given basin "b" calculated from data of cruise "c" is formally defined as:

$$I_{b,c}^{C_{ant}} = \sum_{l=1}^{k} \rho_{b,l,c} \cdot C_{ant}^{b,l,c} \cdot Th_{b,l,c} \quad (1)$$

where the index "k" is the total number of layers found under the track of cruise "c" in basin "b". $C_{ant}^{b,l,c}$ stands for the average concentration of C_{ant} of layer "l" in basin "b" during cruise "c" (Table 2), and "ρ" is the seawater density (in kg m^{-3}). In order to consider the spatiotemporal variability of the "Th" term in Eq. (1) the following expressions are used:

$$F_{b,l,c} = \frac{\%Th_{b,l,c}^{obs}}{\%Th_{b,l,c}^{WOA05}} = \frac{Th_{b,l,c}^{obs} / \sum_{l=1}^{k} Th_{b,l,c}^{obs}}{Th_{b,l,c}^{WOA05} / \sum_{l=1}^{k} Th_{b,l,c}^{WOA05}} \quad (2)$$

$$Th_{b,l,c} = Th_{b,l}^{WOA05} \cdot F_{b,l,c} \quad (3)$$

As stated earlier, the factor $F_{b,l,c}$ in Eq. (2) compares the layer thicknesses observed

during the cruises ($Th^{obs}_{b,l,c}$, listed in Table 2a–c) and the ones calculated from WOA05 data along the cruise "c" track section ($Th^{WOA05}_{b,l,c}$, listed in Table 2a–c). So, for instance, $Th^{WOA05}_{ENA,LSW,A16N}$ would stand for the thickness of LSW in the ENA basin as calculated from WOA05 data for the A16N cruise track. Therefore, $F_{b,l,c}$ is a measure of how representative is layer "l" (as observed during cruise "c" in basin "b", i.e., $Th^{obs}_{b,l,c}$) of the average thickness calculated from the climatological data in WOA05. The assumption here is that the factor $F_{b,l,c}$ is constant for a given basin and it varies from layer to layer, which is congruent with our aim of estimating the target variable of layer thickness.

The term $Th^{WOA05}_{b,l}$ in Eq. (3) is listed in Table 2a–c as "WOA05" under the "$Th^{WOA05}_{b,l,c}$" column for each basin "b" and layer "l". It stands for the overall basin average thickness of layer "l" calculated from WOA05 climatology. The expression for $Th_{b,l,c}$ in Eq. (3) serves to scale the $Th^{WOA05}_{b,l}$ accordingly with the degree of representativeness of $Th^{obs}_{b,l,c}$ for the average basin conditions, i.e., $F_{b,l,c}$.

There is a caveat associated with the calculation of "$Th_{b,l,c}$" as in Eq. (3). This formulation does not ensure that $\sum_{l=1}^{k} Th^{obs}_{b,l,c} = \sum_{l=1}^{k} Th^{WOA05}_{b,l,c}$ in all cruises. This is due to the fact that the bathymetries recorded during the cruises may not necessarily coincide with those in the 1°×1° ETOPO2 database that are used in WOA05 related calculations. Therefore, there is yet another minor correction to be done in order to ensure that the integral in Eq. (1) will always be done over the same bottom depth "z" and, therefore, over the same total volume of the basin irrespectively of the considered cruise. The basin standardization factor "$f_{b,c}$" in Eq. (4) provides correction for this effect. This correction applies when calculating either specific inventories (i.e., inventories per unit area) or total inventories, where the volume of the basin is calculated as

the "Area$\cdot \sum_{l=1}^{k} \mathrm{Th}_{b,l,c}$".

$$f_{b,c} = \frac{\sum_{l=1}^{k} \mathrm{Th}_{b,l,c}}{\sum_{l=1}^{k} \mathrm{Th}_{b,l}^{WOA05}} \quad (4)$$

The sum in the numerator of Eq. (4) corresponds to the terms calculated from Eq. (3), while the sum in the denominator can be easily computed by adding up the corresponding "$\mathrm{Th}_{b,l}^{WOA05}$" terms listed in Table 2a–c. Typically, $f_{b,c}$ have values that are close to the unity, meaning that the correction introduced is minor yet necessary from a formal and operational point of view.

Thus, by considering Eqs. (3) and (4) the "$\mathrm{Th}_{b,l,c}$" expression is upgraded to the following form:

$$\mathrm{Th}^{*}_{b,l,c} = \mathrm{Th}_{b,l,c} \cdot \frac{1}{f_{b,c}} \quad (5)$$

Finally, considering Eqs. (1) and (5) the expression used in the present study to calculate C_{ant} inventories evolves to:

$${}^{*}I^{C_{ant}}_{b,c} = \sum_{l=1}^{k} C^{b,l,c}_{ant} \cdot \mathrm{Th}^{*}_{b,l,c} \quad (6)$$

The "$C^{b,l,c}_{ant}$" terms in Eq. (6) are listed in the last columns of Table 2a–c. By doing the inventory calculations using this final expression it is possible to evaluate to higher degrees of accuracy the extent to which changes in both the C_{ant} uptake capacities and the volumetric census of each watermass affect the specific inventory of C_{ant}. The rest of average properties listed in Table 2a–c were calculated analogously to how it was done in Pérez et al. (2008), i.e., by vertically and horizontally integrating the discrete

values of each property within each layer, using the upper and lower layer boundaries (vertical integration) and the lateral ends of the layers in each of the cruise tracks and within each of the basins (horizontal integration).

The large extension of the ENA basin compared to the Irminger and Iceland ones, and the high sampling sparseness obtained after having put together all the considered cruises (Fig. 1a) makes the ENA basin a region deserving careful attention. This characteristic features in the ENA make unfeasible applying a Th correction of the kind proposed in Eq. (5). Therefore, in the case of the ENA, the "$Th_{b,l}^{WOA05}$" is directly applied to calculate inventories in this basin (Eq. 10).

Given the large separation between cruises in the ENA basin and the actual spatial variability of the considered tracers, the observed average layer properties in each cruise can deviate significantly from basin values, so potential biases in C_{ant} are also expected. The latter can be corrected by considering the expectedly co-variances of C_{ant} with the water mass thermohaline and chemical properties (θ and S), and state of ventilation (for which AOU is used as a proxy) with the assumption that the basin averages of θ, S and AOU at the time of the cruise can be well approximated by the WOA05 values. Therefore, in order to make up for this sparseness of data in the wide extension of the ENA basin, the "$C_{ant}^{ENA,l,c}$" terms in Eq. (6) were also optimised $\left({}^{*}C_{ant}^{ENA,l,c}\right)$, so as to obtain more robust inventory estimates. The "$C_{ant}^{ENA,l,c}$" terms were corrected to better represent the C_{ant} values in each considered layer of the ENA basin (Fig. 1b) by adding to the previously calculated "$C_{ant}^{ENA,l,c}$" a new term named as "$\Delta C_{ant}^{ENA,l,c}$" (Eq. 7). This new term represents the deviation of "$C_{ant}^{ENA,l,c}$" at the time the cruise was conducted, from climatological basin averages. The "$\Delta C_{ant}^{ENA,l,c}$" terms will be computed using WOA05 as a reference.

$$ {}^{*}C_{ant}^{ENA,l,c} = C_{ant}^{ENA,l,c} + \Delta C_{ant}^{ENA,l,c} \quad (7) $$

These small "$\Delta C_{ant}^{ENA,l,c}$" biases are expectable because, for each layer, a spatial gradient in C_{ant} exists linked to the different ventilation of the watermasses. Perez et

al. (2008) found in the Irminger basin a clear relationship between AOU and C_{ant} saturation for different water masses. As a matter of fact, the AOU in the ENA basin displays a positive southward gradient in all layers. The elements for bias correction "$\left(\Delta C_{ant}^{ENA,l,c}\right)$" were computed from cruise data and expressed as individual correction elements for each cruise and layer in the ENA basin as follows:

$$\Delta C_{ant}^{ENA,l,c} = \sum_{i=1}^{3} a_i \left(X_i^{WOA05,l,c} - X_i^{ENA,l,c}\right) \quad (8)$$

Where subscript "i" denotes "property", namely: 1=AOU; 2=θ; 3=S. The "X_i^c" and "X_i^{WOA05}" terms are the average magnitudes of the "ith" property from direct observations and from the WOA05 data at the same location of the considered cruise track, respectively (Table 2a–c). The "a_i" factors are the regression coefficients. They are calculated, for each layer, from an MLR fit (Eq. 9) of the C_{ant} averages $\left(C_{ant}^{ENA,l,c}\right)$ vs. the "i" properties (Table 2c) for the eleven available cruises in the ENA basin. The obtained "a_i" regression coefficients are listed in Table 3.

$$^{MLR}C_{ant}^{ENA,l,c} = \sum_{i=1}^{4} a_i X_i^{ENA,l,c} + k \quad (9)$$

All terms and scripts in this $^{MLR}C_{ant}^{ENA,l,c}$ equation have the same meaning as in Eq. (8). Silicate was initially contemplated, but no significant correlations were obtained and it was thus discarded from the fit. The X_4 term is the xCO_2^{atm} for the year of the corresponding cruise "c". The xCO_2^{atm} time series records were obtained from selected meteorological stations of the global cooperative air-sampling network managed and operated by the National Oceanic and Atmospheric Administration (NOAA; http://www.esrl.noaa.gov/gmd/ccgg/flask.html) Carbon Cycle Greenhouse Gas group. It must be noticed that the "a_4" term in Table 3 associated with the xCO_2^{atm} explanatory variable in $^{MLR}C_{ant}^{ENA,l,c}$ is not used in Eq. (8). This is because $\Delta C_{ant}^{ENA,l,c}$ is computed for

each cruise at the same cruise year $\left(X^{\mathrm{WOA05,l,c}}_{x\mathrm{CO_2^{atm}}} = X^{\mathrm{ENA,l,c}}_{x\mathrm{CO_2^{atm}}}\right)$. Such terms are however mandatory when calculating the "a_i" coefficients (Eq. 9; Table 3), since $x\mathrm{CO_2^{atm}}$ has a clear and strong covariation with C_{ant}. Having "a_4" included in the ${}^{\mathrm{MLR}}C^{\mathrm{ENA,l,c}}_{\mathrm{ant}}$ expression removes from the rest of "a_i" factors the transient influences which certainly co-vary with $C^{\mathrm{ENA,l,c}}_{\mathrm{ant}}$. Resultantly, more robust MLR coefficients are obtained.

All C_{ant} values in Table 2c are actually ${}^{*}C^{\mathrm{ENA,l,c}}_{\mathrm{ant}}$, while the ones in Table 2a and b are simply $C^{\mathrm{Irminger,l,c}}_{\mathrm{ant}}$ and $C^{\mathrm{Iceland,l,c}}_{\mathrm{ant}}$, respectively, i.e., the average C_{ant} concentrations in layer "l" from individual C_{ant} estimates obtained after applying the φC_T° method to the data from cruise "c". Thence, the inventories of C_{ant} in the ENA basin will be calculated in the present work according to a slightly modified version of Eq. (6) after Eq. (7), namely:

$$ {}^{*}I^{C_{\mathrm{ant}}}_{\mathrm{ENA,c}} = \sum_{l=1}^{k} {}^{*}C^{\mathrm{ENA,l,c}}_{\mathrm{ant}} \cdot \mathrm{Th}^{\mathrm{WOA05}}_{\mathrm{b,l}} \qquad (10) $$

4 Results and discussion

The potential temperature fields in Fig. 2 and average values in Table 2a show a temperature minimum corresponding to the cLSW layer in the Irminger basin during the early 90' (Table 2a) followed by a warming during the early 2000s. A clear increase in salinity is observed in the LSW that extends over the Irminger and Iceland basins, in agreement with previous studies and observations (Sarafanov et al., 2007; Yashayaev et al., 2008). Except for the TTO cruise, the SPMW in the Iceland basin, over the Reykjaness Ridge (Fig. 1a), appears to have clearly increased its salinity over time (Fig. 2; Table 2b; Thierry et al., 2008). In the Irminger Sea an increase in AOU in the SAIW, uLSW and cLSW layers is observed during the high to low NAO phase transition that started in the late 1990s and produced larger stratification of the water column. The

θ, S, AOU and C_{ant} of some water masses, like the LSW or SPMW, are clearly altered during the stratification period with respect to the distributions of the early 1990s (Fig. 2).

Regarding the C_{ant} concentration fields in Fig. 2, there is a generalised increase of the C_{ant} burdens in the upper layers (SAIW, SMPW and NACW) for the whole domain, evolving from average values of 35–40 µmol kg^{-1} in 1991–1993 to the peak average values (above 55 µmol kg^{-1}) recorded during OVIDE 2006 (Fig. 3). This result was expectable from the increasing atmospheric xCO_2 over time, which went from ~350 ppm in 1991 to ~379 ppm in 2006. The C_{ant} isopleth of 15–20 µmol kg^{-1} demarcates a sharp gradient that separates the low C_{ant} in deep waters from the more ventilated upper and intermediate layers. Interestingly, this isopleth appears to deepen over time (Fig. 2). The increasing of C_{ant} during 1991–1997 in intermediate layers (particularly in LSW) is the result of the high convective activity of the North Atlantic. Conversely, the deeper water masses of the ENA basin (mostly lNADW) show no significant tendencies in their C_{ant} content between 1991 and 2006.

The average θ, S, AOU, $Si(OH)_4$, C_{ant} and layer thicknesses given in Table 2a–c give a general overview of the variability followed by these properties between 1981 and 2006 in the North Atlantic. In the Irminger basin, Pérez et al. (2008) showed the stratification weakening from 1981 (TTO cruise) to 1991 (AR7E cruise) and the minimum reached in 1997 (FOUREX cruise). These events are both due to the spreading of newly formed LSW in the Labrador basin and, to a lesser extent, in the Irminger basin, as it can be corroborated from the increase of the LSW average thickness (Table 2a; Fig. 4a) and the input of highly ventilated, colder and less saline waters (average AOU, θ and S minima; Table 2a).

The enhanced production of LSW fosters a fast injection of C_{ant} into the upper and intermediate layers of the Irminger basin between 1981 and 1997. Although C_{ant} is seen to increase progressively from 1981 through 2006, this does not happen at a steady rate. The trend of rapid C_{ant} increase in the LSW layers observed during 1991–1997 of 0.77±0.07 µmol kg^{-1} yr^{-1} slows down clearly during the OVIDE era (Table 2a, Fig. 3), in

agreement with the results in Pérez et al. (2008). A similar behaviour is seen for uLSW, while SAIW shows a more steady rate from 1981 to 2006 of 0.62±0.03 µmol kg^{-1} yr^{-1}, which is near twice the observed rate of uNADW and DSOW. This same recurring tendency of fast C_{ant} concentration rates of increase during 1991–1997 and the later slowdown during the OVIDE era is observed for the rest of transient tracers studied in the Irminger basin (Kieke et al., 2006).

In the Iceland basin the physical-chemical properties of the surface layers (SPMW) are highly influenced by the upper limb of the MOC, i.e., by the North Atlantic Current (NAC), which generates a west-to-east gradient of increasing θ and S. This explains the higher than basin average values in the SPMW layer for those cruises running close to the eastern boundary of the Iceland basin, along the 20° W (CAOS-1998 and A16N-2003; Fig. 1a). On the contrary, the OACES-1993 cruise recorded θ and S average values below the Iceland basin climatological value (SPMW WOA in Table 2b) mainly due to the increase in advection of Subpolar water caused by the increase in the Subpolar gyre surface transport during high NAO phase periods (Hátún et al., 2005). Alternatively, the high AOU and $Si(OH)_4$ values observed during the FOUREX cruise in 1997 respond to the trajectory of the cruise, which runs close to the southern boundary of the Iceland basin and is therefore more influenced by Antarctic Intermediate Water (AAIW). Regarding C_{ant} in the SPMW, it increases monotonically over time by about 0.70±0.08 µmol kg^{-1} yr^{-1} (Fig. 3) during the whole period.

The thermohaline variability of the uLSW and cLSW in the Irminger basin is rather narrow, but shows certain similarities with the trends described for SPMW. The higher-than-average θ and S for uLSW registered during the CAOS (1998) and A16N (2003) cruises running along 20° W are likely due to a higher presence of SPMW towards the northeast of the basin (Sarafanov et al., 2008). Similar anomalies are observed for AOU and $Si(OH)_4$ in these two cruises, which show the maximum values recorded between 1981 and 2006. Regarding C_{ant}, the uLSW shows a steady increase from 1981 to 2006 of 0.40±0.06 µmol kg^{-1} yr^{-1}, while cLSW shows a clear increase from 1991 to 1998 (~1.1±0.2 µmol kg^{-1} yr^{-1}, which is almost three times the mean rate for

1981–2006) and later stabilises at around 25.6 µmol kg^{-1} until 2006.

The lower layers of the Iceland basin, represented by the uNADW, show a thermohaline variability that runs parallel to that of cLSW between 1981 and 2006. Differently though, the low AOU and $Si(OH)_4$ values from the 20° W cruises reveal a larger contribution of ISOW to the uNADW than for the other cruises, which are more influenced by Antarctic Bottom Water (AABW). Due to the entrainment of ISOW over the Iceland-Scotland sills, strong inputs from the upper layers that occurred between 1981 and 1998 have imprinted a noticeable C_{ant} increase in these deep layers, showing a mean rate of ~0.42±0.09 µmol kg^{-1} yr^{-1} for 1981–2006. When the strong convection period relaxed afterwards, this trend of C_{ant} increase also weakened and yielded a noisier pattern in C_{ant} increase tendencies.

In the upper layers of the ENA basin the observed thermohaline trends for the NACW are not as well defined as in the upper layers of the other two basins. However, the high convection events, corresponding to 1990–1993 and 1998 with minimum of AOU, are likely linked with rapid responses in this region to the NAO shifts. Most cruises in the ENA were conducted south of the basin and thus the values of θ, S and AOU in Table 2c for NACW are generally higher than the WOA05. The C_{ant} storage rate in this layer are the highest ones for the North Atlantic (average 1.13±0.14 µmol kg^{-1} yr^{-1}; Table 2c) and show a clear increase over the whole 1981–2006 time interval (Fig. 3c).

The cruises that sampled the south of the ENA basin show the highest salinity values, which correspond to the MW layer (Table 2c). For instance, the BD3 (1989) cruise that covered the northwest region of the Iberian Peninsula, close to the MW formation area, has the maximum salinity values, similar to FOUREX in 1997. The opposite occurs for the A01E (1991) cruise. The AOU values for the MW layer are quite high compared to the climatological value (WOA05), and they are modulated by the degree of dilution of MW. There is a general increase in average C_{ant} concentrations of 0.32±0.02 µmol kg^{-1} yr^{-1}. In spite of the correction of the uneven spatial coverage applied through Eq. (7), some bias remains (Fig. 3c): for instance, cruises conducted along of 20° W tend to have lower C_{ant} values than the rest of cruises.

The high AOU and $Si(OH)_4$ values are good indicators of how the presence of LSW in the ENA basin fades progressively towards the Iberian Peninsula, where the BD3 shows the LSW θ and S maximum values, those properties being quite homogeneous throughout the rest of the basin (Table 2c). The low AOU signal in 1991 and 1993 stems from the far-reaching spreading of LSW caused after the strong convection period that occurred during that time (Read and Gould, 1992; Sy et al., 1997). For the ENA basin a quite constant rate of C_{ant} increase ($0.34\pm0.03\,\mu mol\,kg^{-1}\,yr^{-1}$) is found for the LSW throughout the whole 1981–2006 time interval.

The warm component of NADW (uNADW) is less influenced by AABW than the cold component (lNADW), which is reflected by the low $Si(OH)_4$ values of the former compared with those of the latter. The higher influence of LSW/ISOW in the uNADW is revealed by its imprint in the AOU and $Si(OH)_4$ values, which are the lower than observed in the lNADW layer. The patterns of the average C_{ant} concentrations in these two water masses are similar: they are the lowest ones found in the study area and no significant trends of increase are detected. Having found the lowest concentration of C_{ant} in these two very old water masses is an indicator of how good are both the accuracy of the φC_T° method (Vázquez-Rodríguez et al., 2009a) and of the average C_{ant} calculation methodology outlined in Sect. 3.

The $C_{ant}^{Irminger,l,c}$, $C_{ant}^{Iceland,l,c}$ and ${}^*C_{ant}^{ENA,l,c}$ averages presented in Table 2 are plotted in Fig. 3, together with the temporal trends of C_{ant} specific inventories, which were calculated as described in the preceding section from Eqs. (6) and (10). In the Irminger basin, the obtained results are similar to those in Pérez et al. (2008), i.e., there is a large decadal variability in the C_{ant} storage rates of change. During the early 1990's, the rate of change in the total inventory of C_{ant} ($0.013\pm0.002\,Gt\,yr^{-1}$) is almost twice the average for 1981–2006, whilst a remarkable drop to almost half this value ($0.006\pm0.002\,Gt\,yr^{-1}$) followed from 1997 onwards, mostly due to the lower contribution from the LSW, which is the most influential water mass in the Irminger Sea. The NAO shift from a positive to a negative phase in 1996 led to a reduction of the air-sea heat loss in the Labrador Sea. The consequent convection weakening accompanied

by a stratification increase caused the overall weakening of the northern North Atlantic CO_2 sink reported in several works (Corbiere et al., 2007; Schuster et al., 2007; Perez et al., 2008), which contributes significantly to accelerate the increase of atmospheric CO_2 levels during the present decade (Le Quéré et al., 2009).

The latter argumentation linking the contribution of LSW and the variability of C_{ant} total inventories is consistent with the temporal variability of layer thicknesses ($Th^*_{b,l,c}$; Eq. 5) shown in Fig. 4a. It is indeed observed that the volumetric census of cLSW reaches a peak during the first half of the 1990s. Interestingly, the thickness of the uLSW is out of phase with respect to the cLSW thickness peaks (Fig. 4a). Also, the development of the uNADW appears to follow that of the uLSW, suggesting that the volumetric census of this deeper layer is modulated by the strength of the convective activity in the Labrador Sea and Irminger basin too, which ultimately determines the extent of cLSW formation.

During the early nineties the strong convection processes in the Labrador and Irminger Sea (Yashayaev et al., 2008) favoured the transformation of some uLSW (upper 1000 m) and uNACW (below 1500 m) into cLSW. The latter transformation and the increase of advected cLSW support also a downstream increase (from the Irminger towards the Iceland basin) of the mixing between uNACW and cLSW, thus reducing the uNACW thickness. During low convection periods the cLSW penetration gets reduced and the mixing favours the thickening of uLSW and uNADW at expenses of cLSW, in both the Irminger and Iceland basins. The lower C_{ant} concentrations of the uNACW compared to those in cLSW lead to larger C_{ant} inventories when the thickness of LSW increases with respect to the uNACW one. The uLSW and cLSW have similar C_{ant} concentrations and therefore affect the variability of C_{ant} inventories to lesser extents through variations of their respective thicknesses.

Thus, from the above, the differences in North Atlantic C_{ant} storage rates between high and low NAO phases are attributable to the changes in C_{ant} concentrations and also to the decrease in the LSW volumetric census during the low NAO phase of 1997–2006 (Fig. 4b) rather than on an actual decrease in the amount of C_{ant} stored in the

various water masses in this basin (Steinfeldt et al., 2009). This can be stated since inventories were calculated considering the temporal variability of thickness (Eq. 6; Table 2b).

The undersampling in the ENA basin together with the high spatial variability of the specific inventories masks the temporal trends that might have contributed to the observed changes of C_{ant} specific inventories driven mainly by shifts in the NAO phase. At the moment, our best estimate does not reveal any evident link between the NAO phase and the C_{ant} inventory rates of change in the ENA. By considering the same high and low NAO periods as in the Iceland Basin and applying Eq. (10) to calculate the specific inventories of C_{ant}, we obtained almost identical specific storage rates for the ENA basin, namely: $0.019_5 \pm 0.002$ (R^2=0.98) and 0.019 ± 0.005 (R^2=0.87) Gt yr^{-1} for the high and low NAO periods, respectively. This is why a single storage rate for the whole 1981–2006 time period is calculated in the case of the ENA basin, i.e., 0.019 ± 0.001 Gt yr^{-1} (Table 4).

The C_{ant} storage rates of in each basin were calculated by considering the areas of the three basins given in Fig. 5. Since this was done over the entire time period of study, the changes in the C_{ant} storage rates per basin and for the whole study area (the "OVIDE BOX"; Fig. 5) can be obtained and compared for the high and low NAO phase periods. These calculations together with the specific inventory rates (purple lines in Fig. 3) are summarised in Table 4.

Very few studies can be used as benchmarks for our C_{ant} storage rates estimates in Table 4. Álvarez et al. (2004) or Mikaloff-Fletcher et al. (2006) provide some indirect calculations to compare with. The latter mentioned studies have used C_{ant} transport and inventory estimates to calculate C_{ant} uptake rates from the atmosphere in "closed-box" type models for large oceanic regions, such as the North Atlantic. Álvarez et al. (2004) computed a constant C_{ant} storage rate of 0.07 ± 0.03 Gt C yr^{-1} for a region that is similar to the OVIDE box (Fig. 5), but with the FOUREX cruise as the southern bound of the box. This estimate, rescaled to our OVIDE box (considering the areas involved) would amount up to 0.044 ± 0.020 Gt C yr^{-1}, which is between our estimates

of 0.054±0.006 Gt C yr^{-1} (Table 4) during high NAO scenarios and 0.026±0.003 Gt during the low NAO phases. On the other hand, Mikaloff-Fletcher et al. (2006) have calculated for the region enclosed between 49° N and 76° N a constant C_{ant} storage rate of 0.11±0.01 Gt C yr^{-1}. Applying the same scaling as for the result in Álvarez et al. (2004) and omitting the Nordic Seas, which alone represent 0.017 Gt C yr^{-1} (Jutterström et al., 2008) in terms of C_{ant} storage rate, the Mikaloff-Fletcher et al. (2006) estimate for the OVIDE box would map to 0.065±0.002 Gt C yr^{-1}. It must be recalled that the works from Álvarez et al. (2004) and Mikaloff-Fletcher et al. (2006) both used a constant MPD approximation to calculate their steady-state C_{ant} storage rates.

Lherminier et al. (2007) brings forward that in our study area the intensity of the transport associated with the MOC does not vary significantly from high to low NAO phases (19.2±0.9 and 16.9±1.0 Sv, respectively). Knowingly of this behaviour, a quasi-stationary state for the water mass transports within the upper limb of the MOC in the OVIDE box can be roughly assumed. Therefore, by considering: a) the horizontal C_{ant} transports calculated in either Álvarez et al. (2004) or Mikaloff-Fletcher et al. (2006) of 0.04 and 0.02 Gt C yr^{-1}, respectively, and b) the C_{ant} inventories calculated in our work, then the C_{ant} uptake rates from the atmosphere in low NAO phase scenarios would actually be strongly reduced or even positive, meaning that anthropogenic CO_2 outgasing from the ocean could be witnessed in the North Atlantic. This result encourages even more conducting and putting together joint studies in the future that will examine simultaneously C_{ant} storage, transports and air-sea CO_2 fluxes in this region. Such research efforts will be assets to better understand and accurately assess the behaviour of the North Atlantic as an anthropogenic CO_2 source or sink in the future.

5 Conclusions

There is a generalised increase in C_{ant} burdens in the upper layers of the North Atlantic in response to the increasing atmospheric xCO_2 over time. The C_{ant} increase in

intermediate layers (particularly LSW) is the result of the deep convective activity in the Subpolar North Atlantic that occurred during the first half of the 90s.

In the Irminger basin, the C_{ant} storage rates respond to changes in the NAO phase. During the early 1990's, the rate of change in C_{ant} specific inventories ($0.013 \pm 0.002\,Gt\,yr^{-1}$) is almost twice the average for 1981–2006, whilst a remarkable drop to almost half that rate ($0.006 \pm 0.002\,Gt\,yr^{-1}$) followed from 1997 onwards, mostly due to smaller LSW contributions. In the Iceland basin, the differences between high and low NAO phases in the C_{ant} specific inventory rates are even larger than in the Irminger. The reason for it is two-folded: On the one hand, a decrease in the LSW volumetric census during the low NAO phase (1997–2006) has been observed. Adding to that, there exists a slowdown in the rates of C_{ant} being stored in the uLSW and cLSW on a yearly basis during that same time period. Alternatively, the NADW in the Iberian basin showed negligible changes in their C_{ant} storage rates, while NACW stores the largest C_{ant} concentrations of the NASPG and increases its storage capacity faster than any other of the considered water masses, on a yearly basis ($1.13 \pm 0.14\,\mu mol\,kg^{-1}\,yr^{-1}$).

The overall results show that, in the "OVIDE BOX", the C_{ant} storage rates during the high NAO phase from 1991–1997 are ~48% higher than during the low NAO phase that followed for 1997–2006 (Table 4), pointing towards a decrease in the strength of the North Atlantic sink of atmospheric CO_2. The changes in C_{ant} storage rates here obtained are in good agreement with results from Corbiere et al. (2007) and Schuster et al. (2007), who found analogous decreasing rates in the air-sea CO_2 from surface fCO_2 measurements in the North Atlantic.

Acknowledgements. This work was developed and funded by the OVIDE research project from the French research institutions IFREMER and CNRS/INSU, by the European Commission within the 6th Framework Programme (EU FP6 CARBOOCEAN Integrated Project, Contract no. 511176), and by the Spanish research project M4AO (Modelo Multiparamétrico de mistura das masas de agua oceánicas PGIDIT07PXIB402153PR). We would like to extend our gratitude to the chief scientists, scientists and the crew who participated and put their efforts in the oceanographic cruises utilized in this study, particularly to those responsible for the carbon,

CFC, and nutrient measurements. Marcos Vázquez-Rodríguez is funded by Consejo Superior de Investigaciones Científicas (CSIC) I3P predoctoral grant program REF.: I3P-BPD2005.

References

Álvarez, M., Pérez, F. F., Bryden, H. L., and Ríos, A. F.: Physical and biogeochemical transports structure in the North Atlantic subpolar gyre, J. Geophys. Res., 109, C03027, doi:10.1029/2003JC002015, 2004.

Azetsu-Scott, K., Jones, E. P., Yashayaev, I., and Gershey, R. M.: Time series study of CFC concentrations in the Labrador Sea during deep and shallow convection regimes (1991–2000), J. Geophys. Res., 108(C11), 3354, doi:10.1029/2002JC001317, 2003.

Böning, C. W., Scheinert, M., Dengg, J., Biastoch, A., and Funk, A.: Decadal variability of subpolar gyre transport and its reverberation in the North Atlantic overturning, Geophys. Res. Lett., 33, L21S01, doi:10.1029/2006GL026906, 2006.

Bradshaw, A., Brewer, P., Shafer, D., and Williams, R.: Measurements of total carbon dioxide and alkalinity by potentiometric titration in the geosecs program, Earth Planet. Sc. Lett., 55, 99–115, 1981.

Broecker, W. S., Takahashi, T., Simpson, H. J., and Peng, T. H.: Fate of fosil fuel carbon dioxide and the global carbon budget, Science, 206, 409–418, 1979.

Bryden, H. L., Longworth, H. R., and Cunningham, S. A.: Slowing of the Atlantic meridional overturning circulation at 25° N, Nature, 438, 655–657, 2005.

Clayton, T. D. and Byrne, R. H.: Calibration of m-cresol purple on the total hydrogen ion concentration scale and its application to CO_2-system characteristics in seawater, Deep-Sea Pt. I, 40, 2115–2129, 1993.

Corbière, A., Metzl, N., Reverdin, G., Brunet, C., and Takahashi, T.: Interannual and decadal variability of the oceanic carbon sink in the North Atlantic subpolar gyre, Tellus, 59, 1–11, doi:10.1111/j.1600-0889.2006.00232, 2007.

Curry, R., McCartney, M. S., and Joyce, T. M.: Oceanic transport of subpolar climate signals to mid-depth tropical waters, Nature, 391, 575–577, 1998.

Dickson, A. G.: The measurement of sea water pH, Mar. Chem., 44, 131–142, 1993a.

Dickson, A. G.: pH buffers for sea water media based on the total hydrogen ion concentration scale, Deep-Sea Res., 40, 107–118, 1993b.

Dickson, R. R., Lazier, J. R. N., Meincke, J., Rhines, P. B., and Swift, J. H.: Long-term coordinated changes in the convective activity of the North Atlantic, Prog. Oceanogr., 38, 241–295, 1996.

Dickson, R. R., Yashayaev, I., Meincke, J., Turrell, B., Dye, S., and Holfort, J.: Rapid freshening of the deep North Atlantic Ocean over the pastfour decades, Nature, 416, 832–837, 2002.

DOE: Handbook of the Methods for the Analysis of the Various Parameters of the Carbon Dioxide System in Sea Water, Version 2, ORNL/CDIAC-74, edited by: Dickson, A. G. and Goyet, C., 1994.

Drijfhout, S. S. and Hazeleger, W.: Changes in MOC and gyre-induced Atlantic Ocean heat transport, Geophys. Res. Lett., 33, L07707, doi:10.1029/2006GL025807, 2006.

Friis, K., Koertzinger, A., Patsch, J., and Wallace, D. W. R.: On the temporal increase of anthropogenic CO_2 in the subpolar North Atlantic, Deep-Sea Res. Pt. I, 52, 681–698, 2005.

Häkkinen, S. and Rhines, P. B.: Decline of the subpolar North Atlantic circulation during the 1990s, Science, 204, 555–559, 2004.

Hátún, H., Sandø, A. B., Drange, H., Hansen, B., and Valdimarsson, H.: Influence of the Atlantic subpolar gyre on the thermohaline circulation, Science, 309, 1841–1844, 2005.

Holfort, J., Johnson, K. M., Schneider, B., Siedler, G., and Wallace, D. W. R.: Meridional transport of dissolved inorganic carbon in the South Atlantic Ocean, Global Biochem. Cy., 12(3), 479–499, 1998.

IPCC: Summary for Policymakers, in: Climate Change 2007: Impacts, Adaptation and Vulnerability. Contribution of Working Group II to the Fourth Assessment Report of the Intergovernmental Panel on Climate Change, Cambridge University Press, Cambridge, UK, 7–22, http://ipcc-wg1.ucar.edu/wg1/wg1-report.html, 2007.

Johnson, K. M., Wills, K. D., Butler, D. B., Johnson, W. K., and Wong C. S.: Coulometric total carbon dioxide analysis for marine studies: Maximizing the performance of an automated continuous gas extraction system and coulometric detector, Mar. Chem., 44, 167–189, 1993.

Jutterström, S., Jeansson, E., Anderson, L. G., Bellerby, R., Jones, E. P., Smethie, W. M., and Swift, J. F.: Evaluation of anthropogenic carbon in the Nordic Seas using observed relationships of N, P and C versus CFCs, Prog. Oceanogr., 78, 78–84, 2008.

Keeling, C. D. and Bolin, B.: The simultaneous use of chemical tracers in oceanic studies, Tellus, 19, 566–581, 1967.

Kieke, D., Rhein, M., Stramma, L., Smethie, W. M., LeBel, D. A., and Zenk, W.: Changes in the CFC inventories and formation rates of Upper Labrador Sea Water, 1997–2001, J. Phys.

Oceanogr., 36, 64–86, 2006.
Kieke, D., Rhein, M., Stramma, L., Smethie, W. M., Bullister, J. L., and LeBel, D. A.: Changes in the pool of Labrador Sea Water in the subpolar North Atlantic, Geophys. Res. Lett., 34, L06605, doi:10.1029/2006GL028959, 2007.
Latif, M., Böning, C. W., Willebrand, J., Biastoch, A., Dengg, J., Keenlyside, N., and Schweckendiek, U.: Is the thermohaline circulation changing? J. Climate, 19, 4631–4637, 2006.
Lazier, J., Hendry, R., Clarke, R. A., Yashayaev, I., and Rhines, P: Convection and restratification in the Labrador Sea, 1990–2000, Deep-Sea Res., 49, 1819–1835, 2002.
Le Quéré, C., Raupach, M. R., Canadell, J. G., Marland, G. et al.: Trends in the sources and sinks of carbon dioxide, Nat. Geosci., 2, 831–836, doi:10.1038/ngeo689, 2009.
Lherminier, P., Mercier, H., Gourcuff, C., Alvarez, M., Bacon, S., and Kermabon, C.: Transports across the 2002 Greenland-Portugal Ovide section and comparison with 1997, J. Geophys. Res., 112, C07003, doi:10.1029/2006JC003716, 2007.
Mikaloff-Fletcher, S. E., Gruber, N., Jacobson, A. R., Doney, S. C., Dutkiewicz, S., Gerber, M., Follows, M., Joos, F., Lindsay, K., Menemenlis, D., Mouchet, A., Müller, S. A., and Sarmiento, J. L.: Inverse estimates of anthropogenic CO_2 uptake, transport, and storage by the ocean, Global Biogeochem. Cy., 20, GB2002, doi:10.1029/2005GB002530, 2006.
Millero, F. J.: The marine inorganic carbon cycle, Chem. Rev., 107, 308–341, 2007.
Millero, F. J., Zhang, J. Z., Lee, K., and Campbell, D. M.: Titration alkalinity of seawater, Mar. Chem., 44, 153–156, 1993.
Mintrop, L., Perez, F. F., Gonzalez-Davila, M., Santana-Casiano, M. J., and Kortzinger, A.: Alkalinity determination by potentiometry: Intercalibration using three different methods, Cienc. Mar., 26(1), 23–37, 2002.
Ono, T., Watanabe, S., Okuda, K., and Fukasawa, M.: Distribution of total carbonate and related properties in the North Pacific along 30° N, J. Geophys. Res., 103, 30873–30883, 1998.
Pérez, F. F. and Fraga, F.: A precise and rapid analytical procedure for alkalinity determination, Mar. Chem., 21, 169–182, 1987.
Pérez, F. F., Vázquez-Rodríguez, M., Louarn, E., Padín, X. A., Mercier, H., and Ríos, A. F.: Temporal variability of the anthropogenic CO_2 storage in the Irminger Sea, Biogeosciences, 5, 1669–1679, 2008, http://www.biogeosciences.net/5/1669/2008/.
Pierrot, D., Brown, P., Van Heuven, S., Tanhua, T., Schuster, U., Wanninkhof, R., and Key, R. M.: CARINA TCO2 data in the Atlantic Ocean, Earth Syst. Sci. Data Discuss., 3, 1–26, 2010,

http://www.earth-syst-sci-data-discuss.net/3/1/2010/.
Read, J. F. and Gould, W. J.: Cooling and freshening of the subpolar North Atlantic Ocean since the 1960s, Nature, 360, 55–57, 1992.
Roson, G., Rios, A. F., Perez, F. F., Lavin, A., and Bryden, H. L.: Carbon distribution, fluxes, and budgets in the subtropical North Atlantic Ocean (24.5° N), J. Geophys. Res., 108(C5), 3144, doi:10.1029/1999JC000047, 2003.
Sabine, C. L., Feely, R. A., Gruber, N., Key, R. M., Lee, K., Bullister, J. L., Wanninkhof, R., Wong, C. S., Wallace, D. W. R., Tilbrook, B., Millero, F. J., Peng, T.-H., Kozyr, A., Ono, T., and Ríos A. F.: The oceanic sink for anthropogenic CO_2, Science, 305, 367–371, 2004.
Sarafanov, A., Falina, A., Sokov, A., and Demidov, A.: Intense warming and salinification of intermediate waters of southern origin in the eastern subpolar North Atlantic in the 1990s to mid-2000s, J. Geophys. Res., 113, C12022, doi:10.1029/2008JC004975, 2008.
Sarafanov, A., Sokov, A., Demidov, A., and Falina, A.: Warming and salinification of intermediate and deep waters in the Irminger Sea and Iceland Basin in 1997–2006, Geophys. Res. Lett., 34, L23609, doi:10.1029/2007GL031074, 2007.
Sarmiento, J. L. and Le Quéré, C.: Oceanic carbon dioxide uptake in a model of century-scale global warming, Science, 274, 1346–1350, 1996.
Schuster, U. and Watson, A. J.: A variable and decreasing sink for atmospheric CO_2 in the North Atlantic, J. Geophys. Res., 112, C11006, doi:10.1029/2006JC003941, 2007.
Steinfeldt, R., Rhein, M., Bullister, J. L., and Tanhua, T.: Inventory changes in anthropogenic carbon from 1997–2003 in the Atlantic Ocean between 20° S and 65° N, Global Biogeochem. Cy., 23, GB3010, doi:10.1029/2008GB003311, 2009.
Sy, A., Rhein, M., Lazier, J. R. N., Koltermann, K. P., Meincke, J., Putzka, A., and Bersch, M.: Surprisingly rapid spreading of newly formed intermediate waters across the North Atlantic Ocean, Nature, 386, 675–679, 1997.
Tanhua, T., Biastoch, A., Körtzinger, A., Lüger, H., Böning, C., and Wallace, D. W. R.: Changes of anthropogenic CO_2 and CFCs in the North Atlantic between 1981 and 2004, Global Biogeochem. Cy., 20, GB4017, doi:10.1029/2006GB002695, 2006.
Tanhua, T., Olsson, K. A., and Jeansson, E.: Tracer evidence of the origin and variability of Denmark Strait OverflowWater, in: Arctic-Subarctic Ocean Fluxes: Defining the role of the Nordic Seas in Climate, edited by: Dickson, R. R., Meincke, J., and Rhines, P., Springer Verlag, 475–503, 2008.
Thierry, V., de Boisséson, E., and Mercier, H.: Interannual variability of the subpolar mode water

properties over the Reykjanes Ridge during 1990–2006, J. Geophys. Res., 113, C04016, doi:10.1029/2007JC004443, 2008.

Vázquez-Rodríguez, M., Padin, X. A., Ríos, A. F., Bellerby, R. G. J., and Pérez, F. F.: An upgraded carbon-based method to estimate the anthropogenic fraction of dissolved CO_2 in the Atlantic Ocean, Biogeosciences Discuss., 6, 4527–4571, 2009a, http://www.biogeosciences-discuss.net/6/4527/2009/.

Vázquez-Rodríguez, M., Touratier, F., Lo Monaco, C., Waugh, D. W., Padin, X. A., Bellerby, R. G. J., Goyet, C., Metzl, N., Ríos, A. F., and Pérez, F. F.: Anthropogenic carbon distributions in the Atlantic Ocean: data-based estimates from the Arctic to the Antarctic, Biogeosciences, 6, 439–451, 2009b, http://www.biogeosciences.net/6/439/2009/.

Velo, A., Perez, F. F., Brown, P., Tanhua, T., Schuster, U., and Key, R. M.: CARINA alkalinity data in the Atlantic Ocean, Earth Syst. Sci. Data, 1, 45–61, 2009a, http://www.earth-syst-sci-data.net/1/45/2009/.

Velo, A., Pérez, F. F., Lin, X., Key, R. M., Tanhua, T., de la Paz, M., van Heuven, S., Jutterstrm, S., and Ríos, A. F.: CARINA data synthesis project: pH data scale unification and cruise adjustments, Earth Syst. Sci. Data Discuss., 2, 421–475, 2009b, http://www.earth-syst-sci-data-discuss.net/2/421/2009/.

Yashayaev, I., Penny Holliday, N., Bersch, M., and van Aken, H. M.: The history of the Labrador Sea water: production, spreading, transformation and loss, in: Arctic-Subarctic Ocean Fluxes: Defining the Role of the Northern Seas in Climate, edited by: Dickson, R. R., Meincke, J., and Rhines, P., Springer, The Netherlands, 569–612, 2008.

Yashayaev, I., van Aken, H. M., Holliday, N. P., and Bersch, M.: Transformation of the Labrador Sea Water in the subpolar North Atlantic, Geophys. Res. Lett., 34, L22605, doi:10.1029/2007GL031812, 2007.

Table 1. North Atlantic cruises (Fig. 1). P.I.=Principal Investigator; n.a.=no adjustment made. The adjustments from an a posteriori crossover analysis are given in µmol kg^{-1} for C_T and A_T and in pH units for pH (Pierot et al., 2009; Velo et al., 2009a,b).

	Cruise information					Adjustments		
Section	Year	P.I.	Expocode	# Stations	# Samples	pH	C_T	A_T
TTO	1981	T. Takahashi	316N19810923	30	591	n.a.	−3.0	−3.6
BD3	1989	M. Arhan	35LU19890509	20	218	0.024	n.a.	n.a.
Tyro	1990	G. Fransz	64TR19900417	11	189	n.a.	n.a.	14
AR07E	1991	H. M. van Aken	64TR19910408	30	616	n.a.	6	n.a.
A01E	1991	J. Meincke	06MT18_1	26	431	n.a.	n.a.	n.a.
Oaces	1993	R. Wanninkhof	OACES93	28	497	n.a.	n.a.	n.a.
FOUREX	1997	S. Bacon	74DI19970807	83	1458	−0.005	n.a.	n.a.
MET97	1997	F. Schott	06MT19970707	8	148	n.a.	n.a.	n.a.
CHAOS	1998	Smythe – Wright	74DI19980423	26	459	0.018	n.a.	−8.5
OVIDE '02	2002	H. Mercier	35TH20020611	85	1829	n.a.	n.a.	n.a.
A16N	2003	J. Bullister – N. Gruber	33RO20030604	25	693	n.a.	n.a.	n.a.
OVIDE '04	2004	T. Huck	35TH20040604	98	2091	n.a.	n.a.	n.a.
OVIDE '06	2006	P. Lherminier	06M220060523	89	1937	n.a.	n.a.	n.a.

Table 2a. Temporal evolution between 1981 and 2006 of the average values (±standard error of the estimate, i.e., $\pm\sigma/\sqrt{N}$, where N=number of data) salinity (S), potential temperature (θ), apparent oxygen utilization (AOU), silicate ($Si(OH)_4$) and C_{ant} for the water masses considered in the Irminger basin (2a), the Iceland basin (2b) and the ENA basin (2c). In the case of Thickness (Th), the standard deviation is given instead of the standard error of the estimate. The acronyms "I" and "c" stand for "layer" and "cruise", respectively. The "Obs" acronym in the second "Thickness" column stands for "observed" from cruise measurements. The WOA05 climatological values are given as references. The WOA05 term in the "Year" column represents the climatological basin conditions calculated from WOA05 data. Whenever a year is listed more than once it is because more than one cruise was conducted in this particular basin, for example, the 1997 cruises FOUREX and MET97 in the Irminger basin (Table 2a).

Year	$Th^{WOA05}_{Irminger,I,c}$ (m)	$Th^{obs}_{Irminger,I,c}$ (m) (m)	Salinity	θ (°C)	AOU ($\mu mol\,kg^{-1}$)	Silicate ($\mu mol\,kg^{-1}$)	$C^{Irminger,I,c}_{ant}$ ($\mu mol\,kg^{-1}$)
SAIW (σ_0<27.68 kg m^{-3})							
1981	497±126	425±116	34.894±0.002	5.370±0.006	18.6±0.3	7.96±0.09	29.2±1.5
1991	496±87	144±161	34.981±0.002	5.228±0.010	19.0±0.5	8.50±0.15	34.6±2.5
1991	494±71	303±60	34.962±0.001	5.482±0.004	25.8±0.2	8.96±0.05	35.2±0.9
1997	427±67	468±98	34.911±0.001	5.902±0.005	27.9±0.2	7.69±0.07	38.7±1.2
1997	371±43	414±45	34.893±0.001	5.134±0.003	30.1±0.2	8.83±0.05	38.9±0.8
2002	452±47	405±35	34.949±0.001	5.362±0.004	24.6±0.2	8.08±0.06	41.1±0.9
2004	456±44	556±40	34.967±0.001	5.611±0.003	23.8±0.1	7.93±0.04	44.2±0.7
2006	445±36	564±33	34.977±0.001	5.660±0.003	24.1±0.1	7.88±0.04	44.1±0.6
WOA05	**434±12**	*	34.964±0.004	5.544±0.027	19.7±0.3	7.89±0.04	*
uLSW (27.68<σ_0<27.76 kg m^{-3})							
1981	555±72	823±102	34.865±0.001	3.534±0.004	28.1±0.2	9.28±0.07	25.2±1.1
1991	581±61	713±78	34.889±0.001	3.577±0.004	24.2±0.2	9.52±0.07	31.3±1.1
1991	567±41	616±35	34.900±0.001	3.728±0.003	28.7±0.2	10.05±0.05	28.4±0.8
1997	600±37	515±47	34.877±0.001	3.533±0.005	35.6±0.3	9.67±0.08	31.2±1.3
1997	588±33	506±26	34.869±0.001	3.520±0.003	35.9±0.1	10.17±0.04	32.8±0.7
2002	587±34	686±36	34.896±0.001	3.803±0.003	35.0±0.1	9.30±0.04	32.7±0.6
2004	588±36	673±51	34.888±0.001	3.710±0.003	37.2±0.1	9.50±0.04	33.1±0.7
2006	590±39	637±36	34.902±0.001	3.831±0.002	34.4±0.1	9.48±0.04	35.0±0.6
WOA05	**358±17**	*	34.925±0.002	3.997±0.020	33.5±0.2	9.62±0.04	*
cLSW (27.6<σ_0<27.81 kg m^{-3})							
1981	875±75	557±63	34.917±0.002	3.375±0.008	39.1±0.4	10.58±0.12	18.6±2.0
1991	747±67	970±94	34.879±0.001	3.137±0.003	32.6±0.2	10.16±0.05	24.6±0.8
1991	791±71	869±81	34.881±0.001	3.156±0.003	29.8±0.1	10.30±0.04	25.6±0.7
1997	933±98	988±142	34.871±0.001	2.986±0.004	31.1±0.2	9.94±0.06	29.7±1.0
1997	802±67	983±80	34.868±0.001	2.989±0.003	30.9±0.1	10.43±0.04	29.9±0.7
2002	810±30	678±43	34.897±0.001	3.184±0.003	38.8±0.2	10.23±0.05	26.2±0.8
2004	828±28	546±41	34.902±0.001	3.232±0.004	40.5±0.2	10.44±0.06	27.7±0.9
2006	828±28	535±28	34.923±0.001	3.369±0.003	40.8±0.2	10.58±0.05	27.8±0.8
WOA05	**453±25**	*	34.899±0.001	3.314±0.012	35.7±0.1	10.25±0.03	*
uNADW (27.81<σ_0<27.88 kg m^{-3})							
1981	466±54	686±104	34.948±0.001	2.980±0.005	44.3±0.2	12.01±0.07	14.1±1.2
1991	498±42	746±82	34.940±0.001	2.925±0.003	48.4±0.2	12.66±0.05	12.9±0.8
1991	472±54	667±84	34.935±0.001	2.887±0.003	44.9±0.2	12.79±0.05	15.3±0.8
1997	525±63	516±60	34.917±0.001	2.785±0.005	41.5±0.3	11.26±0.08	20.0±1.3
1997	670±58	754±78	34.924±0.001	2.813±0.004	44.2±0.2	12.81±0.06	20.0±1.0
2002	540±54	762±64	34.918±0.001	2.759±0.003	43.7±0.1	11.50±0.04	19.7±0.7
2004	532±59	755±69	34.916±0.001	2.753±0.003	44.4±0.1	11.70±0.04	22.6±0.7
2006	551±55	745±75	34.930±0.001	2.859±0.003	43.2±0.1	11.70±0.04	23.0±0.7
WOA05	**275±9**	*	34.915±0.003	2.869±0.028	42.7±0.2	11.30±0.10	*
DSOW (σ_0>27.88 kg m^{-3})							
1981	47±28	98±28	34.892±0.002	1.679±0.008	36.7±0.4	9.80±0.12	12.7±2.0
1991	105±35	134±35	34.897±0.001	1.778±0.005	41.6±0.3	10.20±0.08	12.7±1.4
1991	291±24	86±24	34.896±0.001	1.794±0.006	38.1±0.3	10.57±0.09	15.5±1.5
1997	242±36	90±36	34.897±0.002	1.772±0.009	38.0±0.5	9.73±0.14	20.5±2.3
1997	151±28	94±28	34.894±0.002	1.720±0.008	38.8±0.4	11.11±0.13	20.1±2.1
2002	144±21	110±21	34.887±0.001	1.721±0.005	39.4±0.3	9.53±0.08	17.7±1.3
2004	167±26	112±26	34.869±0.001	1.535±0.005	36.3±0.2	8.92±0.07	21.9±1.1
2006	158±31	126±31	34.906±0.001	1.874±0.004	37.7±0.2	9.77±0.07	22.4±1.1
WOA05	**56±123**	*	34.895±0.004	1.885±0.064	40.1±0.2	11.08±0.19	*

Table 2b. Continued.

Year	$Th^{WOA05}_{Iceland,I,c}$ (m)	$Th^{obs}_{Iceland,I,c}$ (m) (m)	Salinity	θ (°C)	AOU ($\mu mol\,kg^{-1}$)	Silicate ($\mu mol\,kg^{-1}$)	$C^{Iceland,I,c}_{ant}$ ($\mu mol\,kg^{-1}$)
SPMW (σ_0<27.60 kg m^{-3})							
1981	438±61	889±91	35.183±0.001	8.242±0.003	28.2±0.1	6.89±0.04	25.8±0.7
1991	764±56	694±49	35.109±0.001	7.030±0.003	22.9±0.2	7.73±0.05	34.4±0.8
1991	974±53	531±35	35.000±0.002	6.935±0.007	37.8±0.3	8.94±0.10	37.4±1.7
1993	691±23	840±36	35.151±0.001	7.889±0.003	31.6±0.1	6.68±0.04	39.7±0.7
1997	475±31	535±41	35.094±0.001	7.931±0.003	47.2±0.2	8.17±0.05	39.5±0.8
1998	668±25	864±30	35.249±0.001	8.563±0.003	28.7±0.2	7.22±0.05	41.1±0.8
2002	619±22	647±38	35.117±0.001	7.614±0.003	30.5±0.2	7.33±0.05	42.2±0.8
2003	729±33	803±31	35.260±0.001	8.826±0.002	37.4±0.1	6.68±0.03	44.3±0.5
2004	618±18	555±17	35.105±0.001	7.719±0.002	38.5±0.1	7.40±0.04	43.5±0.6
2006	629±21	576±22	35.077±0.001	7.906±0.003	38.7±0.1	7.20±0.04	44.2±0.7
WOA05	**636±13**	*	35.175±0.002	7.954±0.027	29.6±0.4	7.36±0.04	*
uLSW (σ_0>27.60 kg m^{-3}; σ_1<32.35 kg m^{-3})							
1981	868±78	535±59	34.982±0.001	4.637±0.005	48.5±0.3	10.56±0.08	19.1±1.3
1991	548±27	602±21	34.959±0.001	4.488±0.004	56.2±0.2	10.87±0.06	21.1±0.9
1991	767±34	559±24	34.944±0.001	4.340±0.006	51.7±0.3	11.16±0.09	23.0±1.5
1993	581±25	463±15	34.987±0.001	4.754±0.004	56.0±0.2	10.43±0.06	23.2±1.1
1997	549±32	472±26	34.940±0.001	4.345±0.003	55.7±0.2	11.11±0.05	27.2±0.8
1998	618±23	479±27	35.009±0.002	4.938±0.007	62.2±0.3	11.72±0.10	24.2±1.7
2002	508±22	512±24	34.976±0.001	4.657±0.003	57.5±0.2	10.60±0.05	25.3±0.9
2003	455±37	512±43	35.024±0.001	4.979±0.004	63.7±0.2	11.24±0.06	26.0±1.0
2004	504±24	595±40	34.948±0.001	4.408±0.002	55.7±0.1	10.68±0.04	27.9±0.6
2006	506±22	568±21	34.956±0.001	4.494±0.003	54.4±0.1	10.74±0.04	30.3±0.7
WOA05	**360±14**	*	35.015±0.002	4.924±0.001	54.1±0.3	10.79±0.05	*
cLSW (σ_1>32.35 kg m^{-3}; σ_2<37.00 kg m^{-3})							
1981	632±113	650±136	34.943±0.001	3.517±0.004	44.7±0.2	12.13±0.07	17.2±1.1
1991	784±78	826±68	34.928±0.001	3.376±0.003	45.6±0.1	11.59±0.04	15.8±0.7
1991	1879±157	1038±127	34.923±0.001	3.308±0.005	43.5±0.3	12.31±0.08	18.9±1.3
1993	400±114	454±124	34.926±0.001	3.458±0.005	44.6±0.2	11.27±0.07	20.4±1.2
1997	1324±67	1302±72	34.905±0.001	3.170±0.002	40.1±0.1	11.72±0.04	23.4±0.6
1998	326±98	411±138	34.919±0.002	3.372±0.006	44.1±0.3	12.08±0.09	26.0±1.6
2002	1139±121	919±97	34.920±0.001	3.273±0.003	43.1±0.1	11.06±0.04	23.5±0.7
2003	361±88	446±118	34.926±0.001	3.387±0.005	45.2±0.3	11.79±0.08	27.1±1.3
2004	1164±65	971±58	34.909±0.001	3.226±0.003	43.8±0.1	11.32±0.04	24.7±0.6
2006	1179±76	1001±70	34.919±0.001	3.297±0.003	42.2±0.1	11.39±0.04	26.9±0.6
WOA05	**529±23**	*	34.936±0.001	3.414±0.012	45.1±0.1	11.67±0.05	*
uNADW (σ_2>37.00 kg m^{-3}; σ_4<45.84 kg m^{-3})							
1981	159±68	236±86	34.970±0.002	2.732±0.007	52.9±0.3	10.74±0.10	10.7±1.7
1991	199±26	328±37	34.972±0.001	2.762±0.004	53.0±0.2	14.66±0.05	12.6±0.9
1991	760±147	505±157	34.963±0.001	2.718±0.005	55.2±0.2	18.44±0.07	13.3±1.2
1993	86±32	87±22	34.971±0.003	2.816±0.012	49.3±0.6	12.95±0.18	15.5±3.1
1997	690±76	537±66	34.949±0.001	2.689±0.004	50.0±0.2	15.53±0.06	17.2±1.0
1998	150±85	55±55	34.967±0.004	2.749±0.017	49.7±0.9	13.69±0.26	19.5±4.4
2002	459±45	426±36	34.964±0.001	2.704±0.004	52.8±0.2	15.52±0.05	17.9±0.9
2003	72±56	113±65	34.975±0.003	2.833±0.012	48.3±0.6	13.51±0.18	23.8±3.1
2004	430±67	339±67	34.959±0.001	2.675±0.004	56.0±0.2	17.09±0.06	17.1±1.0
2006	479±15	469±15	34.964±0.001	2.705±0.003	53.2±0.2	17.54±0.05	19.7±0.8
WOA05	**149±15**	*	34.963±0.004	2.710±0.025	56.5±0.3	18.77±0.77	*

Table 2c. Continued.

Year	$Th^{WOA05}_{ENA,I,c}$ (m)	$Th^{obs}_{ENA,I,c}$ (m)	Salinity	θ (°C)	AOU (μmol kg^{-1})	Silicate (μmol kg^{-1})	$C^{ENA,I,c}_{ant}$ (μmol kg^{-1})
NACW (σ_0<27.20 kg m^{-3})							
1981	477±35	459±33	35.618±0.001	12.472±0.003	27.5±0.2	3.74±0.05	34.6±0.9
1989	422±108	439±88	35.661±0.001	12.448±0.004	23.6±0.2	2.86±0.06	38.5±1.0
1990	451±83	454±53	35.668±0.001	12.160±0.003	19.7±0.1	3.52±0.04	41.3±0.7
1991	172±27	334±25	35.532±0.004	11.163±0.015	22.5±0.8	4.66±0.23	43.1±3.8
1993	436±22	436±26	35.544±0.001	11.500±0.004	23.0±0.2	3.02±0.07	44.7±1.1
1997	508±9	495±12	35.673±0.000	12.375±0.002	31.6±0.1	3.58±0.03	48.1±0.5
1998	505±32	470±23	35.659±0.001	12.293±0.002	20.9±0.1	3.62±0.03	46.8±0.5
2002	445±21	456±21	35.643±0.000	12.170±0.002	26.1±0.1	3.58±0.03	51.3±0.5
2003	503±33	457±27	35.657±0.000	12.492±0.002	25.1±0.1	3.47±0.03	52.0±0.5
2004	473±19	463±11	35.637±0.000	12.116±0.002	28.5±0.1	3.63±0.03	51.7±0.5
2006	481±17	455±10	35.659±0.000	12.146±0.002	24.1±0.1	3.43±0.03	56.2±0.5
WOA05	**256±5**	*	35.552±0.004	11.832±0.029	17.9±0.3	3.47±0.02	*
MW (σ_0>27.20 kg m^{-3}; σ_1<32.35 kg m^{-3})							
1981	1006±57	837±47	35.408±0.001	7.812±0.003	72.4±0.1	10.29±0.04	24.4±0.7
1989	1025±52	1026±22	35.745±0.001	9.679±0.003	74.4±0.2	9.34±0.05	31.4±0.8
1990	1007±87	1083±77	35.250±0.001	7.156±0.004	64.2±0.2	10.07±0.05	27.2±0.9
1991	1211±61	739±71	35.107±0.001	6.650±0.003	54.1±0.2	10.07±0.05	28.0±0.9
1993	977±28	1068±34	35.242±0.001	7.125±0.003	64.9±0.1	9.08±0.04	27.9±0.7
1997	958±17	944±18	35.509±0.000	8.413±0.002	75.4±0.1	9.77±0.02	30.7±0.4
1998	887±30	1020±32	35.323±0.001	7.542±0.003	74.6±0.2	10.46±0.05	27.2±0.8
2002	956±12	952±13	35.490±0.000	8.262±0.001	74.2±0.1	9.66±0.02	31.4±0.4
2003	865±22	1050±15	35.365±0.001	7.771±0.002	78.5±0.1	10.21±0.03	28.2±0.6
2004	952±12	947±15	35.456±0.000	8.038±0.001	75.2±0.1	9.86±0.02	31.0±0.4
2006	930±12	967±13	35.493±0.000	8.218±0.001	75.1±0.1	9.76±0.02	34.0±0.4
WOA05	**791±15**	*	35.395±0.004	8.176±0.037	60.2±0.7	9.28±0.05	*
LSW (σ_1>32.35 kg m^{-3}; σ_2<37.00 kg m^{-3})							
1981	981±88	884±78	35.057±0.001	3.975±0.004	56.0±0.2	15.15±0.06	14.4±1.0
1989	634±89	565±49	35.107±0.001	4.353±0.006	62.7±0.3	16.90±0.09	17.7±1.5
1990	598±136	1123±116	35.002±0.002	3.712±0.006	54.5±0.3	14.41±0.10	16.9±1.6
1991	1222±77	960±37	34.920±0.001	3.286±0.004	45.4±0.2	13.21±0.06	17.3±1.0
1993	1051±53	1082±58	34.946±0.001	3.422±0.004	47.2±0.2	12.33±0.05	18.6±0.9
1997	1069±41	985±31	34.997±0.001	3.673±0.002	55.0±0.1	15.27±0.03	20.1±0.6
1998	1052±48	1220±63	34.962±0.001	3.515±0.004	50.2±0.2	13.94±0.05	20.6±0.9
2002	1047±30	1192±25	34.990±0.000	3.636±0.002	51.9±0.1	14.01±0.03	20.6±0.4
2003	1145±55	1200±45	34.957±0.000	3.466±0.003	52.6±0.2	13.60±0.05	18.9±0.8
2004	1068±26	1175±21	34.986±0.000	3.606±0.002	53.0±0.1	14.01±0.02	21.1±0.4
2006	1051±34	1151±24	34.989±0.000	3.642±0.002	50.7±0.1	13.54±0.03	23.6±0.4
WOA05	**511±22**	*	34.990±0.005	3.673±0.031	55.4±0.4	14.99±0.13	*
uNADW (σ_2>37.00 kg m^{-3}; σ_4<45.84 kg m^{-3})							
1981	879±144	731±144	34.947±0.001	2.610±0.005	71.7±0.2	30.40±0.07	7.8±1.2
1989	831±220	1072±220	34.959±0.001	2.738±0.005	74.7±0.3	31.98±0.08	9.7±1.3
1990	584±128	1018±128	34.947±0.002	2.571±0.009	75.9±0.5	32.14±0.14	12.5±2.3
1991	812±86	513±86	34.943±0.001	2.574±0.004	68.5±0.2	28.34±0.06	9.1±1.1
1993	805±55	929±55	34.945±0.001	2.585±0.006	69.4±0.3	28.53±0.08	9.7±1.4
1997	741±64	831±64	34.944±0.001	2.597±0.003	76.3±0.1	32.62±0.04	8.0±0.7
1998	880±67	934±67	34.941±0.001	2.564±0.005	72.6±0.2	31.22±0.07	9.7±1.2
2002	1054±30	1072±30	34.948±0.000	2.611±0.002	71.9±0.1	30.97±0.03	10.0±0.4
2003	748±89	973±89	34.938±0.001	2.515±0.005	77.3±0.2	31.52±0.07	10.1±1.2
2004	1049±25	1111±25	34.943±0.000	2.588±0.002	73.8±0.1	31.17±0.03	9.8±0.4
2006	1028±31	1100±31	34.950±0.000	2.626±0.002	70.5±0.1	30.81±0.03	11.8±0.5
WOA05	**549±28**	*	34.944±0.001	2.589±0.013	77.9±0.2	33.02±0.32	*
lNADW (σ_4>45.84 kg m^{-3})							
1981	859±223	285±156	34.907±0.001	2.151±0.006	85.2±0.3	43.67±0.09	5.9±1.5
1989	539±205	640±150	34.905±0.001	2.130±0.005	85.2±0.3	44.98±0.08	8.5±1.3
1990	382±149	879±135	34.909±0.002	1.964±0.009	90.3±0.4	44.37±0.13	5.0±2.2
1991	178±113	77±91	34.910±0.002	2.182±0.008	87.5±0.4	44.53±0.11	5.8±1.9
1993	659±92	659±72	34.915±0.001	2.193±0.005	84.5±0.3	42.31±0.08	7.0±1.4
1997	647±143	424±113	34.904±0.001	2.131±0.003	87.4±0.2	44.33±0.05	3.6±0.8
1998	729±98	539±98	34.911±0.001	2.180±0.005	87.0±0.2	43.98±0.07	6.5±1.2
2002	899±85	566±45	34.911±0.001	2.158±0.002	86.0±0.1	44.54±0.03	6.6±0.5
2003	679±152	548±132	34.912±0.001	2.192±0.005	85.6±0.2	42.05±0.07	7.9±1.2
2004	875±79	618±67	34.906±0.001	2.149±0.002	87.0±0.1	44.12±0.03	5.8±0.5
2006	942±93	581±73	34.914±0.001	2.159±0.002	85.2±0.1	45.53±0.03	7.2±0.6
WOA05	**321±17**	*	34.908±0.001	2.101±0.046	88.7±0.5	42.96±0.63	*

Table 3. List of coefficients obtained for Eq. (8) using the expression given in Eq. (9) for each layer in the ENA basin. The constant terms "k" are not input parameters for Eq. (8) and not reported. The information between brackets in the header line gives the associated "i-th" property and the units of the "a_i" coefficients. The "n.s." acronym stands for "not significant". The variables with this acronym explained very little of the $C_{ant}^{ENA,I,c}$ variability and worsened the overall MLR fit. They were therefore rejected according to a stepwise method of MLR solving.

Eastern North Atlantic (ENA) Basin					
Layer	R^2	a_1 (AOU; kg µmol^{-1})	a_2 (θ; °C^{-1})	a_3 (S)	a_4 (xCO$_2$; ppm^{-1})
NACW	0.97	n.s.	n.s.	n.s.	0.47±0.03
MW	0.96	−0.31±0.05	n.s.	17±2	0.18±0.02
LSW	0.90	−0.38±0.20	n.s.	n.s.	0.19±0.02
uNADW	0.64	n.s.	−65±22	(0.7±0.2)×10^3	0.06±0.03
lNADW	0.02	−0.52±0.22	n.s.	n.s.	n.s.

Table 4. The C_{ant} storage rates (±std. err. of the estimate) are given for different time intervals, according to the phases of the North Atlantic Oscillation (NAO).

Basin	NAO Phase (time period)	C_{ant} specific inventory rates (mol C m^{-2} yr^{-1})	Storage rate (kmol s^{-1})	Storage rate (Gt yr^{-1})
Irminger	High (1991–1997)	1.74±0.24	34±5	0.013±0.002
	Low (1997–2006)	0.4±0.3	8±6	0.006±0.002
Iceland	High (1991–1998)	1.88±0.45	57±14	0.022±0.005
	Low (1997–2006)	0.3±0.2	9±6	0.0035±0.003
ENA	(1981–2006)	0.72±0.03	51±2	0.019±0.001
Total	High NAO	1.18±0.12	142±15	0.054±0.006
(Ovide box)	Low NAO	0.56±0.07	68±9	0.026±0.003

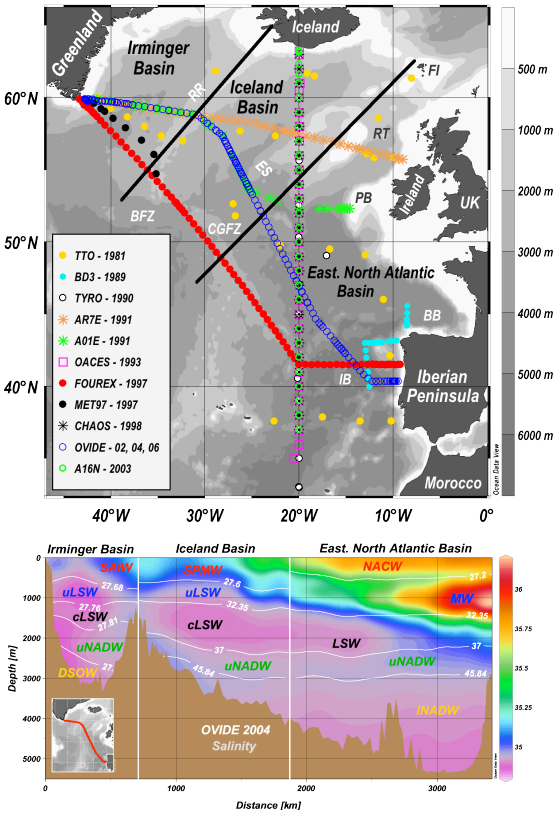

Fig. 1. **(a)** Shows the tracks of the thirteen cruises used in this study, spanning twenty-seven years of marine carbon system measurements. The greyscale on the sidebar indicates depth (m). The two black straight lines are the boundaries selected to distinguish and designate the Irminger, Iceland and ENA basins. Some of the TYRO stations are inevitably masked under the CHAOS, OACES and A16N cruise symbol sets. Acronyms for the underwater and coastal topography denote the following: RR=Reykjanes Ridge; BFZ=Bight Fracture Zone; CGFZ=Charlie-Gibbs Fracture Zone; ES=Eriador Seamount; FI=Faroe Islands; RT=Rockall Trough; PB=Porcupine Bank; BB=Biscay Basin; IB=Iberian Basin. **(b)** Displays the observed salinity field for the OVIDE '04 section, which representatively covers the latitudinal and longitudinal ranges of the studied region. The selected boundary isopycnals (potential density "σ", in kg m^{-3}) used to demarcate and follow the C_{ant} evolution of the main water masses in the Irminger, Iceland and ENA basins are also shown. Surface is generally taken as the reference pressure level for the isopycnals (σ_0, ref. press.=0 dbar), except for the intermediate and deep waters on the Iceland and ENA basins, where 1000, 2000 and 4000 dbar are the references for the σ_1=32.35; σ_2=37.00 and σ_4=45.84 kg m^{-3} isopycnals, respectively. Water mass acronyms mean the following: SAIW=Sub Arctic Intermediate Water; LSW=Labrador Sea Water; NADW=North Atlantic Deep Water; SPMW=Sub Polar Mode Water; NACW=North Atlantic Central Water; MW=Mediterranean Water. The lowercase first letters "c", "u" and "l" denote the "classical", "upper" and "lower" varieties in some water masses, respectively.

BGD
7, 165–202, 2010

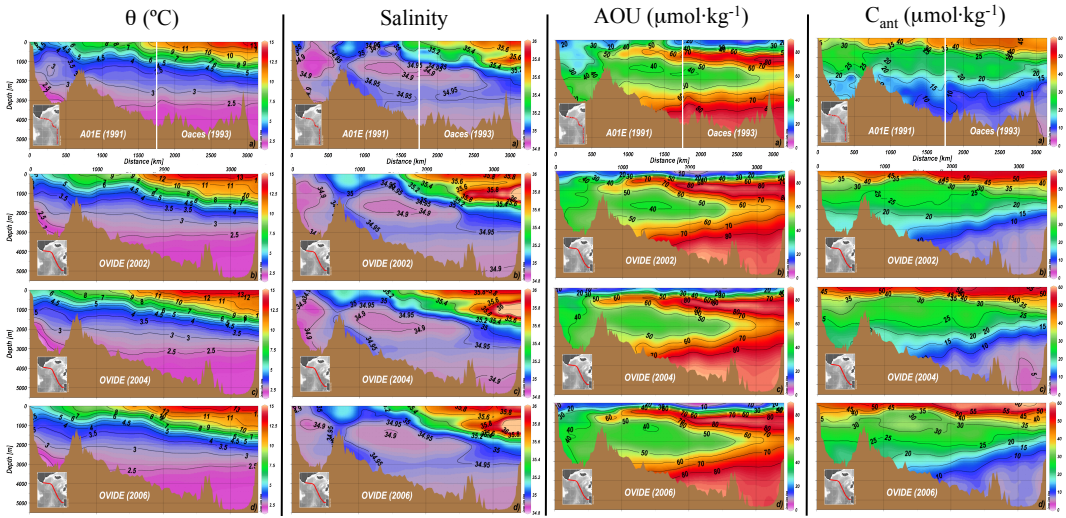

Fig. 2. Contour plots of θ, Salinity, AOU and C_{ant} spanning from 1991 to 2006. The x-axis gives the track distances (km) from the southernmost tip of Greenland towards the Iberian Basin. The top row section is a composite from the A01E and OACES cruises, in order to get the closest match possible with the OVIDE section. Notice that the selected A01E leg perfectly overlaps with the OVIDE tracks. This was done in order to extend directly comparable measurements and C_{ant} estimates of the OVIDE project further back in time by nearly a decade and get a better track of the storage trends. Compared with the nine-year gap between this composite section and the first OVIDE cruise in 2002, the temporal difference between the A01E and OACES cruises is negligible and affordable. On the top composite sections, the continuum fields at the insertion point of the upper, intermediate and deep waters corroborate this assumption and validate the combination of results.

BGD
7, 165–202, 2010

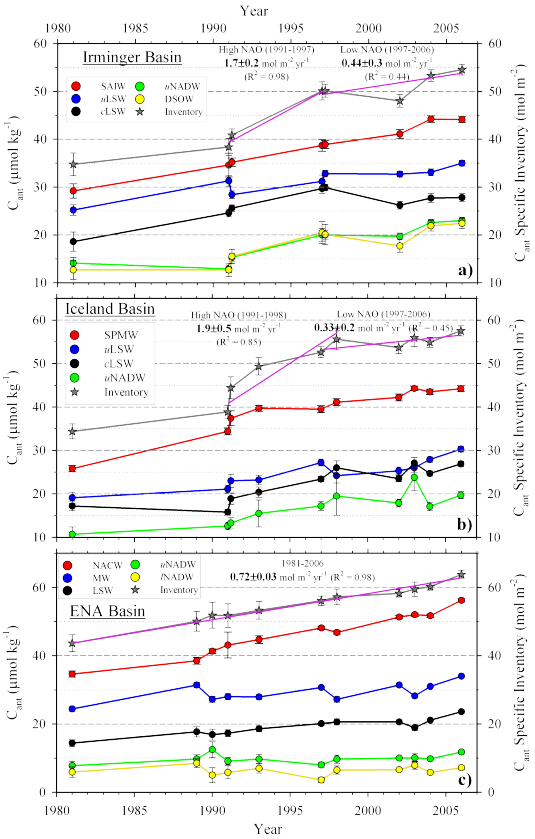

Fig. 3. Trends of average C_{ant} concentrations in the studied water masses at the Irminger **(a)**, Iceland **(b)** and ENA **(c)** basins. Notice that the *y*-axis scale is ad hoc for each graph. The grey lines give the specific inventories, and the purple fit lines stand for the rates of change of the specific inventories (slope and R^2 given for the high and low NAO index periods, except for the ENA basin). The error bars represent the standard error of the mean.

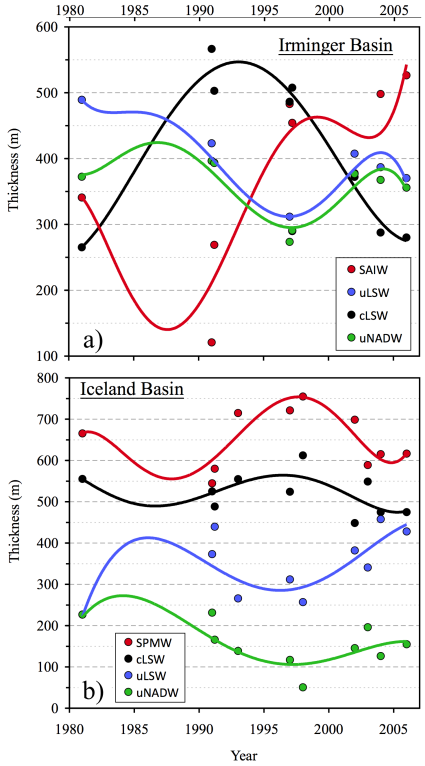

Fig. 4. Scatter plots with overlaid polynomial fits of different orders showing the temporal evolution of layer thicknesses in the Irminger **(a)** and Iceland **(b)** basins. The thicknesses were calculated as given by Eq. (5). The Iceland basin shows a thicker, more developed cLSW layer than in the Irminger basin given the deeper bathymetry of the former one and also because cLSW forms mainly in the Irminger, but develops further towards the Iceland basin. The propagation of Irminger formed waters into the Iceland basin is also the reason for the slight temporal delay observed for the cLSW peak in the Iceland basin (towards 1997) with respect to the Irminger basin (where it occurs around 1993).

BGD
7, 165–202, 2010

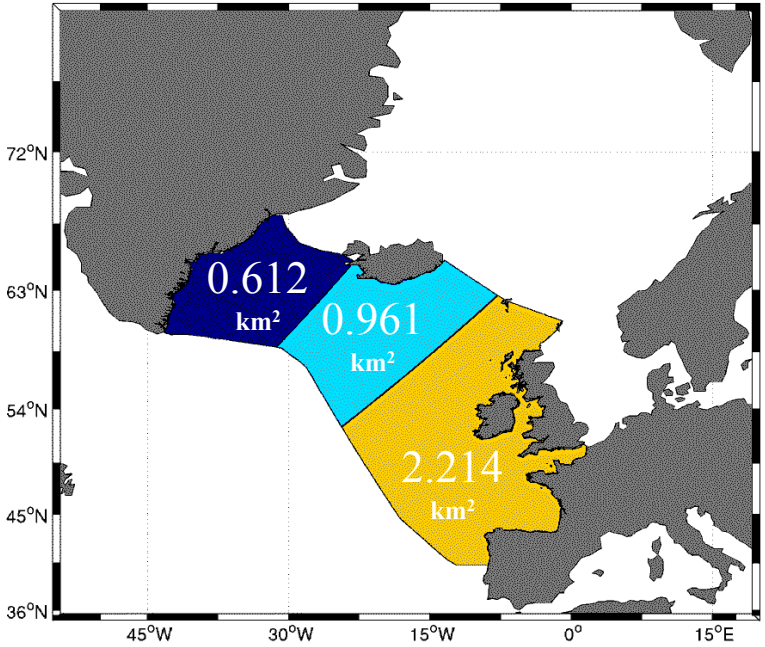

Fig. 5. Areas (in 10^6 km^2) of the Irminger (dark blue), Iceland (indigo blue) and ENA (yellow) basins enclosed by the "OVIDE BOX". These areas were used in the calculation of C_{ant} storage rates from the specific inventory estimates in Fig. 3. The northern geographical boundaries of the "OVIDE BOX" are defined by the North Atlantic sills east and west from Iceland (according to the ETOPO2 bathymethry), while the southern one is delimited by the tracks of the OVIDE cruises.